

THEA-Code: an Autoencoder-Based IDS-correcting Code for DNA Storage

Alan J.X. Guo*, Mengyi Wei, Yufan Dai, Yali Wei, Pengchen Zhang

July 30, 2024

Abstract

The insertion, deletion, substitution (IDS) correcting code has garnered increased attention due to significant advancements in DNA storage that emerged recently. Despite this, the pursuit of optimal solutions in IDS-correcting codes remains an open challenge, drawing interest from both theoretical and engineering perspectives. This work introduces a pioneering approach named THEA-code. The proposed method follows a heuristic idea of employing an end-to-end autoencoder for the integrated encoding and decoding processes. To address the challenges associated with deploying an autoencoder as an IDS-correcting code, we propose innovative techniques, including the differentiable IDS channel, the entropy constraint on the codeword, and the auxiliary reconstruction of the source sequence. These strategies contribute to the successful convergence of the autoencoder, resulting in a deep learning-based IDS-correcting code with commendable performance. Notably, THEA-Code represents the first instance of a deep learning-based code that is independent of conventional coding frameworks in the IDS-correcting domain. Comprehensive experiments, including an ablation study, provide a detailed analysis and affirm the effectiveness of THEA-Code.

1 Introduction

DNA storage, a method that utilizes the synthesis and sequencing of DNA molecules for information storage and retrieval, has attracted significant attention [1–8]. Due to the involvement of biochemical procedures, the DNA storage pipeline can be viewed as an insertions, deletions, or substitutions (IDS) channel [9] over 4-ary sequences with the alphabet $\{A, T, G, C\}$. Consequently, an IDS-correcting encoding/decoding method plays a key role in DNA storage. However, despite its crucial role, the IDS-correcting code is not extensively researched [10], and faces more challenges when applied in DNA storage, such as sequence constraints [11,12], inhomogeneous error distribution [9], *etc.*

Autoencoders, which are extensively researched [13], naturally align with coding theory. Both autoencoders and coding algorithms operate by encoding the input (source) into a feature representation (codeword) and subsequently reconstructing the input (source) through the output (sink) of a decoder [14].

In this study, we aim to employ a heuristic end-to-end autoencoder as the implementation of an IDS-correcting code, referred to as the THEA-Code. The proposed code uses a neural network to encode a source DNA sequence into a longer codeword DNA sequence. After introducing the IDS errors to the codeword, a separate network is employed to decode the codeword into the original source DNA sequence. The immediate challenges associated with implementing such an idea include:

- Applying IDS errors on a sequence is not differentiable, posing a barrier to gradient propagation and hindering the joint training of the autoencoder.
- The feature representations generated by an autoencoder are inherently soft, employing float values, in contrast to the typically hard representations of codewords in coding algorithms, using integer values.
- The complexity of training the model is compounded by the integration of the encoder, channel, and decoder. Furthermore, the different inherent logics of the encoder and decoder aggravate this challenge.

*A.J.G., M.W., Y.D., Y.W., and P.Z. are with the Center for Applied Mathematics, Tianjin University, China. This work was supported by the National Key Research and Development Program of China under Grant 2020YFA0712100. (CONTACT: jiaxiang.guo@tju.edu.cn)

To the best of our knowledge, this work introduces the first end-to-end autoencoder solution for an IDS-correcting code, marking a novel exploration of the first issue in related research. Considering the complexities of the second and third issues, several error-correcting studies have explored alternative approaches. These include the applications of deep learning methods to simulate either a standalone encoder or decoder, as well as specific components of a conventional code [15, 16]. Some researchers have addressed the second issue by incorporating soft power constraints on the binary codeword during pretraining and introducing hard power constraints thereafter [17]. It is noteworthy that all these works are implemented over the white Gaussian noise (AWGN) channel.

Our work builds on addressing these three issues to some extent by introducing the following techniques:

- **Differentiable IDS channel.** A transformer-based model [18] is trained independently to simulate the conventional IDS channel on the unit ℓ_1 sphere. This simulation allows for the propagation of gradients from the channel output.
- **Entropy constraint on the codeword.** As a heuristic approach, we introduce an entropy constraint [19] on the codeword, compelling the probability vectors to be more quantized.
- **Auxiliary reconstruction of source sequence.** We introduce a reconstruction of the source sequence by the output of the encoder. This setup initializes the encoder in the first several training epochs and also ensures that the encoder can provide complete information about the source sequence.

As a result, the proposed THEA-Code converges and reports commendable results. To the best of our knowledge, this is the first end-to-end neural network-based IDS-correcting code, without reliance on any conventional code.

2 Related Works

Many established IDS-correcting codes are rooted in the Varshamov-Tenengolts (VT) code [20], including [11, 21–24]. These codes often rely on rigorous mathematical deduction and provide firm proofs for their coding schemes. However, the stringent hypotheses they use tend to restrict their practical applications. Heuristic IDS-correcting codes for DNA storage, such as those proposed in [25–27], usually incorporate synchronization markers [28, 29], watermarks [30], or positional information [12] within their encoded sequences.

In recent years, deep learning methods have found increasing applications in coding theory [31–33]. Several architectures have been employed as decoders or sub-modules of conventional codes on the AWGN channel. In [34], the authors applied neural networks to replace sub-blocks in the conventional iterative decoding algorithm for polar codes. Recurrent neural networks (RNN) were used for decoding convolutional and turbo codes [16]. Both RNNs and transformer-based models have served as belief propagation decoders for linear codes [15, 35]. Hypergraph networks were also utilized as decoders for block codes in [36]. Despite these advancements, end-to-end deep learning solutions remain relatively less explored. As mentioned in [17], direct applications of multi-layer perceptron (MLP) and convolutional neural network (CNN) are not comparable to conventional methods. To address this, the authors in [17] used deep models to replace sub-modules of a turbo code skeleton, and trained an end-to-end encoder-decoder model. Similarly, in [37], neural networks were employed to replace the Plotkin mapping for the Reed-Muller code. Both of these works inherit frameworks from conventional codes and utilize neural networks as replacements for key modules. In [38], researchers proposed an autoencoder-based inner code with one-bit quantization for the AWGN channel. Confronting challenges arising from quantization, they utilized interleaved training on the encoder and decoder.

3 THEA-Code

3.1 Framework

The flowchart of THEA-Code is depicted in Figure 1. Building on the background of DNA storage, which synthesizes DNA molecules of fixed length, the proposed model is designed to handle source sequences and codewords of immutable lengths. In essence, the proposed method encodes source sequences into codewords; the IDS channel introduces IDS errors to the codewords; and a decoder is engaged to reconstruct the sink sequences according to the corrupted codewords.

Let $f_{\text{en}}(\cdot; \phi)$ represent the deep learning-based encoder, where ϕ denotes the encoder’s parameters. The source sequence \mathbf{s} is firstly encoded into the codeword $\mathbf{c} = f_{\text{en}}(\mathbf{s}; \phi)$ by the encoder.¹ Subsequently, a random error profile \mathbf{p} is generated, which records the positions and types of errors that will occur on codeword \mathbf{c} passing through the IDS channel. Given the error profile \mathbf{p} , the codeword \mathbf{c} is modified into $\hat{\mathbf{c}} = \text{IDS}(\mathbf{c}, \mathbf{p}; \theta)$ by the IDS channel, implemented by a deep model with parameters θ . Throughout the text, we use notations IDS and ids for differentiable and conventional IDS channels, respectively. Finally, a deep decoder $f_{\text{de}}(\cdot; \psi)$ with parameters ψ decodes the corrupted codeword $\hat{\mathbf{c}}$ back into the sink sequence $\hat{\mathbf{s}} = f_{\text{de}}(\hat{\mathbf{c}}; \psi)$.

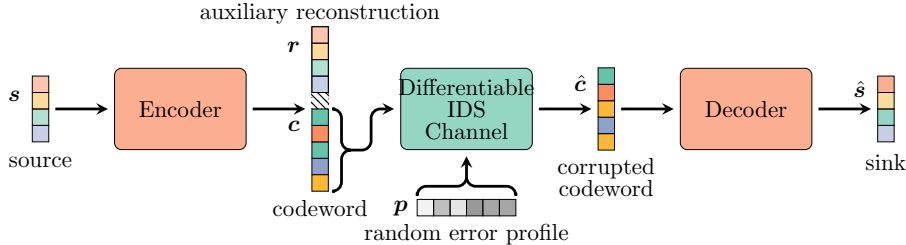


Figure 1: The flowchart of THEA-Code, including the deep learning-based encoder, decoder, and IDS channel.

Following this pipeline, a natural optimization target is the cross-entropy loss

$$\mathcal{L}_{\text{CE}}(\hat{\mathbf{s}}, \mathbf{s}) = - \sum_i \sum_j \mathbb{1}_{j=s_i} \log \hat{s}_{ij}, \quad (1)$$

which evaluates the reconstruction disparity of the source sequence \mathbf{s} by the sink sequence $\hat{\mathbf{s}}$.

However, merely optimizing such a loss function will not yield the desired outcomes. As discussed in Section 1, we propose three techniques to address the emerged challenges, which are differentiable IDS channel, entropy constraint on the codeword, and auxiliary reconstruction of the source sequence.

3.2 Differentiable IDS channel on the unit ℓ_1 sphere

It is evident that the operations of insertion and deletion are not differentiable. Consequently, a conventional IDS channel, denoted as $\text{ids}(\cdot, \cdot)$, which modifies a sequence by directly applying IDS operations, obstructs the gradient propagation and cannot be seamlessly integrated into the autoencoder.

Taking advantage of the logical capabilities inherent in transformer-based models, we employ a sequence-to-sequence model, denoted as $\text{IDS}(\cdot, \cdot; \theta)$, to simulate the conventional IDS channel $\text{ids}(\cdot, \cdot)$. Such a differentiable IDS channel is trained independently before the encoder and decoder. The learned channel $\text{IDS}(\cdot, \cdot; \hat{\theta})$, along with its parameters $\hat{\theta}$, remains fixed during the optimization of the autoencoder.

As depicted in Figure 1, the input \mathbf{c} to the IDS channel is derived from the output of the encoder. After applying softmax, input \mathbf{c} adopts the form of probability vectors, rather than the base types in $\{\text{A}, \text{T}, \text{G}, \text{C}\}$. To align with these probability vectors, we need to promote the IDS operations onto the unit 3-sphere in the ℓ_1 space. For a sequence of probability vectors $\mathbf{c} = (\mathbf{c}_1, \mathbf{c}_2, \dots, \mathbf{c}_k)$, where \mathbf{c}_i is a non-negative vector summing to 1, the insertion operation at index i involves inserting a one-hot vector representing the inserted symbol from the alphabet $\{\text{A}, \text{T}, \text{G}, \text{C}\}$ before index i . Deletion at index i is simply removing the vector \mathbf{c}_i from \mathbf{c} . Regarding substitution, we roll the vector \mathbf{c}_i by corresponding offsets for the three types of substitutions. For example, applying type-1 substitution at index i rolls the original vector $\mathbf{c}_i = (c_{i1}, c_{i2}, c_{i3}, c_{i4})$ to $(c_{i4}, c_{i1}, c_{i2}, c_{i3})$. It is easy to verify that the promoted IDS operations degenerate to plain IDS operations when constraining the probability vectors to one-hot style.

We employ a sequence-to-sequence model, using one-layered transformers for both the encoder and decoder², as the differentiable IDS channel. As illustrated in Figure 2, the model takes the codeword and error profile as its input, by padding the codeword and profile to the same length and concatenating their embeddings along the feature dimension. To generate the output, which represents the corrupted codeword, zero vectors with sinusoidal positional encoding are utilized as the queries (omitted from Figure 2). With these steps, the codeword \mathbf{c} is expected to be modified to $\hat{\mathbf{c}}_{\text{IDS}} = \text{IDS}(\mathbf{c}, \mathbf{p}; \theta)$ according to the error profile

¹For simplicity, we do not distinguish between notations for sequences in letters, one-hot vectors, or probability vectors in the following text.

²The encoder and decoder here both refer to the modules from the sequence-to-sequence model, rather than the modules of the autoencoder. We trust that readers can distinguish them based on the context in similar cases.

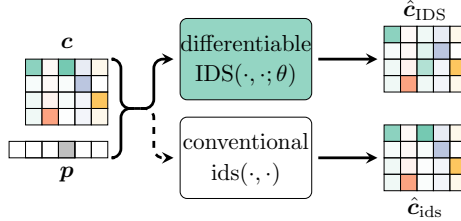


Figure 2: The differentiable IDS channel. The $\hat{\mathbf{c}}_{\text{IDS}}$ and $\hat{\mathbf{c}}_{\text{ids}}$ are generated by the differentiable and conventional IDS channels, respectively. Optimizing the difference between $\hat{\mathbf{c}}_{\text{IDS}}$ and $\hat{\mathbf{c}}_{\text{ids}}$ trains the differentiable IDS channel.

\mathbf{p} . In the lower stream of Figure 2, the codeword \mathbf{c} is modified as $\hat{\mathbf{c}}_{\text{ids}} = \text{ids}(\mathbf{c}, \mathbf{p})$ with respect to the error profile \mathbf{p} using a conventional promoted IDS channel.

To train the model $\text{IDS}(\cdot, \cdot; \theta)$, we can utilize the Kullback–Leibler divergence [39] of $\hat{\mathbf{c}}_{\text{IDS}}$ from $\hat{\mathbf{c}}_{\text{ids}}$

$$\mathcal{L}_{\text{KLD}}(\hat{\mathbf{c}}_{\text{IDS}}, \hat{\mathbf{c}}_{\text{ids}}) = \frac{1}{k} \sum_i \hat{\mathbf{c}}_{\text{ids}i}^T \log \frac{\hat{\mathbf{c}}_{\text{ids}i}}{\hat{\mathbf{c}}_{\text{IDS}i}}. \quad (2)$$

as the optimization target. By optimizing (2) on probability vector sequence \mathbf{c} and randomly generated error profile \mathbf{p} , which are both randomly generated, the parameters θ of the differentiable IDS channel are trained to $\hat{\theta}$. Following this, the model $\text{IDS}(\cdot, \cdot; \hat{\theta})$ simulates the conventional IDS channel $\text{ids}(\cdot, \cdot)$. The significance of such an IDS channel lies in its differentiability. Once optimized independently, the IDS channel has its parameters fixed for subsequent procedures. In the following text, we use $\text{IDS}(\cdot, \cdot)$ to refer to the trained IDS channel for simplicity.

3.3 Entropy constraint on the codeword

As mentioned earlier, a fundamental challenge in applying deep learning methods in the field of coding theory is how to integrate the quantization of outputs into a deep model. This challenge is mainly manifested in the following two aspects.

Firstly, vanilla quantization of a deep model’s output disrupts gradient propagation. To address this, differentiable functions that simulate the arg max function and a mixture of soft and hard functions are potential solutions. For example, out of the scope of coding theory, researchers have directly copied the gradient during training, as in [40]. In [41, 42] the Gumbel softmax, which transitions from continuous to discrete by controlling its temperature, is employed in vector quantised-variational autoencoders (VQ-VAE).

Secondly, vanilla quantization of the codeword results in information loss among the floating-point numbers for the decoder. In this work, the codeword \mathbf{c} is represented as probability vectors. These probability vectors carry richer information than one-hot vectors, which enhances the performance of the autoencoder but also poses challenges for decoding discrete codewords during testing. For example, probability vectors like $\mathbf{c}_i = (0.5, 0.25, 0.25, 0)$ may appear in the output of the encoder, and using arg max to quantize the \mathbf{c}_i provides the decoder an out-of-domain input.

Heuristically, we introduce a simple yet effective entropy constraint [19] on the codeword \mathbf{c} in the form of a probability vector. This constraint penalizes probability vectors deviating from the one-hot style. The Shannon entropy [43] of a discrete distribution $P(x)$ represents the average level of “information” associated with the possible outputs of the variable x , and is calculated as follows:

$$H(x) = - \sum_{x \in \mathcal{X}} P(x) \log P(x). \quad (3)$$

It is easy to verify that (3) is non-negative and equals zero only when the random variable produces a certain output. This condition is equivalent to the probability vector being identical to some one-hot vector. Considering this, we define the entropy constraint on the codeword $\mathbf{c} = (\mathbf{c}_1, \mathbf{c}_2, \dots, \mathbf{c}_k)$ as follows³:

$$\mathcal{L}_{\text{EN}}(\mathbf{c}) = - \sum_i \sum_j c_{ij} \log c_{ij}. \quad (4)$$

This constraint is incorporated into the overall optimization target during the training phase.

³We use the notation of a loss function for the entropy constraint because it is integrated into the overall loss during training.

3.4 Auxiliary reconstruction of source sequence by the encoder

Although a typical autoencoder comprises two parts, the encoder and decoder often collaborate on a unified task in most applications. However, in this work, we anticipate that the encoder and decoder should adhere to distinct inherent logics. Particularly, when imposing constraints on the codeword to exhibit more quantization, the joint training of the encoder and decoder resembles a chicken-and-egg dilemma, where the optimization of each relies on the other during the training phase.

To mitigate the impact of this issue, we introduce a supplementary task exclusively for the encoder to initialize it with some basic logical abilities. We expect the encoder and decoder to be alternatively trained from this initial state of the encoder to their respective endpoints during the training phase. A straightforward task for a sequence-to-sequence model is to replicate the input sequence in the output. Such a task also guarantees the model to present all the information from its input sequence without reduction. In light of this, we explore the addition of a reconstruction task to the encoder.

In practice, the encoder is designed to generate a longer sequence, which is then split into the codeword representation \mathbf{c} and a reconstruction \mathbf{r} of the input source sequence, as illustrated in Figure 1. The auxiliary reconstruction loss is defined as the cross-entropy loss:

$$\mathcal{L}_{\text{AUX}}(\mathbf{r}, \mathbf{s}) = - \sum_i \sum_j \mathbb{1}_{j=s_i} \log r_{ij} \quad (5)$$

measuring the difference between the reconstruction \mathbf{r} and the input sequence \mathbf{s} .

Considering that the auxiliary loss is not expected to have negative effects on the encoder, we do not use a standalone training stage to optimize the auxiliary loss. Therefore, the auxiliary loss (5) is integrated into the overall loss throughout the entire training phase.

It must be mentioned that, despite the strategies discussed in Sections 3.3 and 3.4, careful tuning on the weight for the entropy constraint (3) is essential, as demonstrated in the ablation study.

3.5 The encoder and decoder

The transformer has demonstrated its powerful logical abilities. Drawing inspiration from conventional IDS-correcting codes, which leverage logical and mathematical rules, both the encoder and decoder in our approach are implemented using the transformer-based sequence-to-sequence models.

The encoder and decoder are both (3+3)-layered transformers using sinusoidal positional encoding. The embedding of the DNA bases is implemented through a fully connected layer without bias as the decoder processes probability vectors rather than base types. Learnable embeddings of position indices are used to query the outputs.

3.6 Training phase

The training phase consists of two parts. Firstly, the differentiable IDS channel is fully trained by optimizing:

$$\hat{\theta} = \arg \min_{\theta} \mathcal{L}_{\text{KLD}}(\hat{\mathbf{c}}_{\text{IDS}}, \hat{\mathbf{c}}_{\text{ids}}) \quad (6)$$

on randomly generated codeword \mathbf{c} and profile \mathbf{p} . Once the differentiable IDS channel is trained, its parameters are fixed. The remaining components of the autoencoder are trained by optimizing the weighted summation of (1), (3), and (5):

$$\hat{\phi}, \hat{\psi} = \arg \min_{\phi, \psi} \mathcal{L}_{\text{CE}}(\hat{\mathbf{s}}, \mathbf{s}) + \lambda \mathcal{L}_{\text{EN}}(\mathbf{c}) + \mu \mathcal{L}_{\text{AUX}}(\mathbf{r}, \mathbf{s}), \quad (7)$$

where the λ and μ are hyperparameters representing the corresponding loss weights. The autoencoder is trained on randomly generated input sequences \mathbf{s} .

3.7 Testing phase

In the testing phase, the differentiable IDS channel is replaced with the conventional IDS channel. Firstly, the encoder maps the source sequence \mathbf{s} to the codeword \mathbf{c} in the style of probability vectors. Subsequently, an $\arg \max$ function is applied to translate \mathbf{c} into its letter sequence style, and conventional IDS operations are performed on $\hat{\mathbf{c}} = \text{ids}(\mathbf{c}, \mathbf{p})$ based on a random error profile \mathbf{p} . Following this, the one-hot transformation of $\hat{\mathbf{c}}$ is fed into the decoder, resulting in the production of the sink sequence $\hat{\mathbf{s}}$. Finally, metrics measuring disparities between \mathbf{s} and $\hat{\mathbf{s}}$ are calculated to evaluate the performance of the proposed method.

Since the sequences are randomly generated from an enormous pool of possible terms, we do not distinguish between the training set and the testing set. For instance, in the context of this work, the source sequence is a 100-long 4-ary sequence, providing 1.6×10^{60} candidate sequences. Sets of random sequences have little chance to overlap.

4 Experiments and Ablation Study

Given the scarcity of closely related works for direct comparison, our focus shifts towards conducting ablation studies to provide more insights to the reader. Commonly used methods for synthesizing DNA molecules in DNA storage pipelines typically yield sequences of lengths ranging from 100 to 200. In this study, we choose the number 150 as the codeword length, aligning with these established practices. Unless explicitly stated otherwise, all the following experiments follow the default setting of: source sequence length $\ell_s = 100$, codeword length $\ell_c = 150$, entropy constraint weight $\lambda = 0.01$, and auxiliary loss weight $\mu = 1$. The error profile is generated with a 1% chance of errors occurring at each position, and the probabilities of insertion, deletion, and substitution are equal among the errors.

To evaluate the performance of the proposed method, we employ the nucleobase error rate (NER) as a metric. For a DNA sequence \mathbf{s} and its decoded counterpart $\hat{\mathbf{s}}$, the NER is defined as:

$$\text{NER}(\mathbf{s}, \hat{\mathbf{s}}) = \frac{\#\{s_i \neq \hat{s}_i\}}{\#\{s_i\}}. \quad (8)$$

The NER represents the proportion of nucleobase errors, which corresponds to base substitutions in the source DNA sequence. It’s worth noting that these errors can be post-corrected by a mature conventional outer code.

As aforementioned, the sample set is astronomically large, and we choose not to explicitly separate training, validation, and testing data. All samples used in the training and testing phases are randomly generated. The source code will be made publicly available once this paper is ready for publication. Furthermore, with the aim of designing an IDS-correcting code, we are satisfied with one successful code scheme among several attempts. Consequently, we conduct 5 runs for each setting and report the best result in most cases of experiment settings.

4.1 Performance against coderate

Table 1: The testing NER for different source lengths ℓ_s . The coderate is calculated as ℓ_s/ℓ_c , and the reported NER represents the best result among 5 runs. The source length ℓ_s ranges from 70 to 140, corresponding to coderates that are considered reasonable. The values $\ell_s \in \{150, 160\}$ correspond to coderates not less than 1, which is used to assess whether the model exhibits corruption in such scenarios.

ℓ_s	70	80	90	100	110	120	130	140	150	160
coderate	0.47	0.53	0.60	0.67	0.73	0.80	0.87	0.93	1.00	1.07
NER(%)	0.36	0.50	0.77	1.03	1.37	1.91	2.73	6.07	8.49	12.95

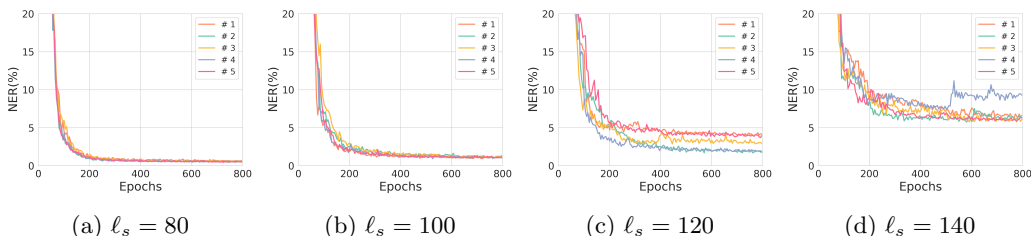


Figure 3: The validation NER across training epochs. For source sequence lengths $\ell_s = 80$ and $\ell_s = 100$, all 5 runs of training show commendable validation performance. For $\ell_s = 120$ and $\ell_s = 140$, certain runs terminate training prematurely, resulting in less competitive results.

The coderate is defined as the proportion of non-redundant data in the codeword, calculated by dividing the source length ℓ_s by the codeword length ℓ_c . In this section, we explore variable source lengths ℓ_s while

keeping the codeword length ℓ_c fixed. Intuitively, lower coderates relieve the burden on the deep model, which is expected to result in better overall performance.

For each coderate ranging from 0.47 to 0.93, we conducted the experiments 5 times and reported the best result in Table 1. As suggested, The results achieve our expectations, revealing a trend where the NER increases from 0.36% to 6.07% along with the enlarged coderate. For curiosity, we also conducted experiments on coderates not less than 1 to investigate whether the autoencoder encounters corruption in these scenarios. The results, which are also presented in Table 1, indicate that the autoencoder maintains its performance. At a coderate of 1, the autoencoder trades roughly 1% IDS errors in the codeword for 8.49% substitution errors, In the case where the source length is 160, the $(160 - 150)/160 = 6.25\%$ NER is instinctive and expected. The numbers suggest that an extra 6.70% NER is introduced by the IDS errors in the codeword in this situation.

In particular, when using a coderate of less than 80%, the NER remains below 2%. By applying an outer conventional error-correcting code to rectify these nucleobase errors in the form of substitutions, a practical IDS-correcting code is achieved. This solution is comparable to existing heuristic IDS-correcting methods in DNA storage [12, 25–27]. We do not present a table comparing the performances, as the heuristic IDS-correcting methods are hard to align under the same experimental setting. For instance, in [12], codewords were duplicated to sequencing depth 5, and decoding was performed on multiple retrieved codewords. As for the mathematically deduced codes mentioned in Section 2, they typically focus on faithfully correcting a single IDS error in the entire codeword or sequence, which is also hard to evaluate in our experiments.

It is also observed that as the coderate increases, the models are more likely to converge to a local minimal point, resulting in numbers that are less competitive across different runs of the same experimental setting. The results are illustrated by the NER against the training epochs in Figure 3. These figures indicate that the models exhibit more diversity when the coderate is increased. For source sequence lengths $\ell_s = 80$ and $\ell_s = 100$, different runs report similar model performance. However, when $\ell_s = 120$ or $\ell_s = 140$, a clear ranking on the different runs in the same setting can be established.

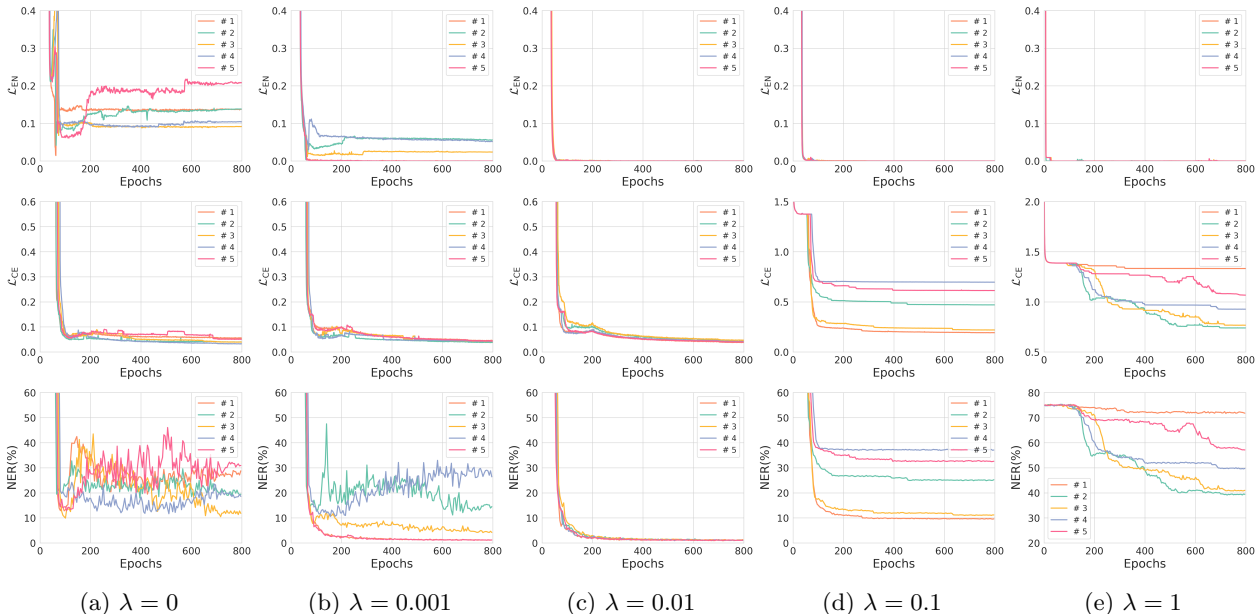


Figure 4: The entropy constraint \mathcal{L}_{EN} , the reconstruction loss \mathcal{L}_{CE} , and the validation NER for various choices of $\lambda \in \{0, 0.001, 0.01, 0.1, 1\}$. Each curve in the subfigures represents one of the 5 runs conducted in the experiment and is plotted against the training epochs.

4.2 Optimization of hyperparameter λ

The hyperparameter λ dictates the weight of the entropy constraint in the overall loss. Imposing the entropy constraint on the codewords compels them to adopt a one-hot style from a probability vector style, which is a double-edged sword. On one hand, this approach, compared to plain quantization, preserves the capability of gradient propagation. Importantly, codewords that closely resemble a one-hot representation mitigate the domain difference between the decoder’s input during the training and the testing phases.

However, the drawback is also non-negligible. If the entropy constraint is overapplied and dominates the model training before the autoencoder is effectively tuned to its intended function, the entropy constraint

may tend to produce a gradient opposite to the loss-propagated gradient, leading the model towards a local minimum convergence point. As a thought experiment, consider a letter $c_i = (0, 0, 0.1, 0.9)$ from a codeword \mathbf{c} where the letter is not aligned with the IDS-correcting aim. The optimization on the reconstruction loss \mathcal{L}_{CE} of (1) may propagate a gradient decreasing the fourth dimension $c_{i4} = 0.9$. However, the entropy constraint on \mathbf{c}_i will faithfully produce an opposite gradient, attempting to increase $c_{i4} = 0.9$ to achieve low entropy, potentially hindering the optimization process.

Fortunately, we discovered that this paradox can be alleviated by careful tuning of the entropy constraint weight. Experiments were conducted with different choices of weight λ in $\{0, 0.001, 0.01, 0.1, 1\}$, and the results are presented in Figure 4. Each column in this figure corresponds to a specific λ value, and the rows depict the entropy \mathcal{L}_{EN} , the reconstruction \mathcal{L}_{CE} loss between $\hat{\mathbf{s}}$ and \mathbf{s} , and the validation NER, from top to bottom.

The first row suggests that the entropy \mathcal{L}_{EN} is controlled by enlarging the constraint weight, while the second row shows that the reconstruction loss \mathcal{L}_{CE} diverges with an overapplied entropy constraint. The third row of NER indicates that the performance is improved by introducing the entropy constraint and worsened by further enlarging the constraint weight.

Column-wise, when using $\lambda = 0$ and $\lambda = 0.001$, the reconstruction \mathcal{L}_{CE} converges well, indicating that the autoencoder is well-trained. However, the entropy on the codeword remains relatively high during the training phase, suggesting that the codewords are diverse from one-hot style. The curves of validation NERs also support this speculation. Although the autoencoder is well-trained, the quantization of the codeword with high entropy alters the input domain for the decoder, and fails the testing phase. Regarding the columns corresponding to $\lambda = 0.1$ and $\lambda = 1$ in Figure 4, we observe that the entropy drops to a low level fast in the first few epochs, and the reconstruction loss \mathcal{L}_{CE} does not decline to an appropriate interval during the training phase. This verifies our conjecture that an overapplied entropy constraint will lead the model to a local minimum convergence point. Overall, the $\lambda = 0.01$ is a proper choice for the constraint weight in our experiments. The model converges well, the entropy maintains at a low level, and the decoder keeps its performance with the quantized codewords.

4.3 Effects of the auxiliary reconstruction loss

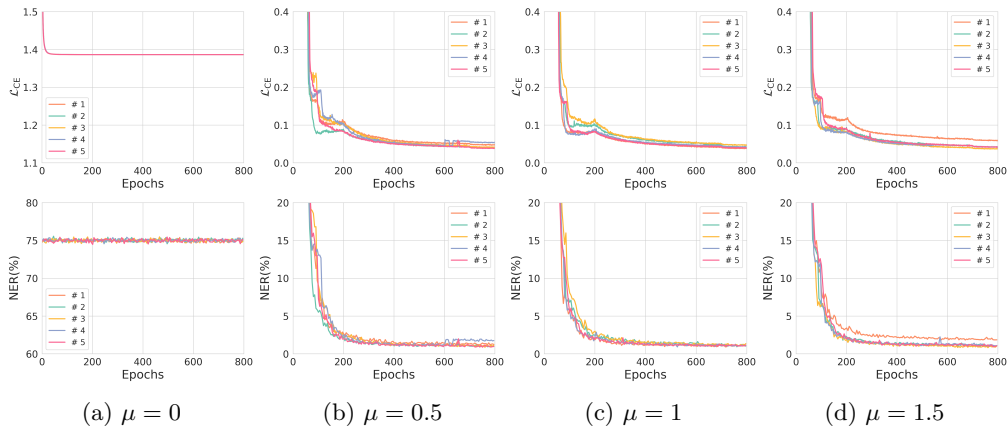


Figure 5: The reconstruction loss \mathcal{L}_{CE} between the source and sink sequences, and the validation NER for various choices of $\mu \in \{0, 0.5, 1, 1.5\}$. Each curve in the subfigures represents one of the 5 runs conducted in the experiment and is plotted against the training epochs.

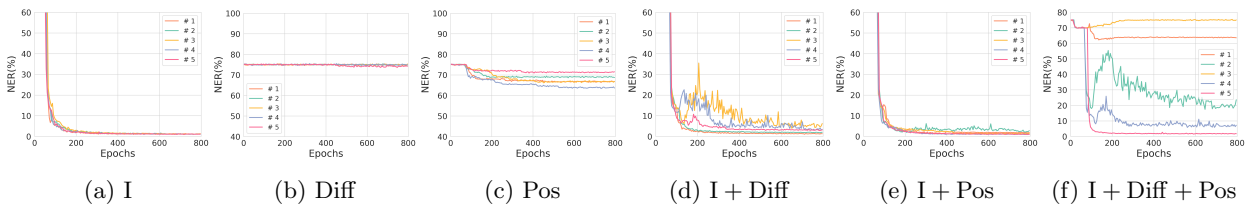


Figure 6: The validation NER against the training epochs with different choices of auxiliary reconstruction. The reconstructed sequences are produced by combinations of the identity mapping I, Diff, and Pos, where + denotes sequence concatenating.

We hypothesized that the encoder and decoder of an error-correcting code follow distinct logics, and the training of each component relies on the maturity of its counterpart. To initialize the training, we introduced the auxiliary reconstruction \mathbf{r} of the source sequence in the output of the encoder, which imparts a basic logical ability to the encoder. In this process, a hyperparameter μ is introduced as the weight of the auxiliary reconstruction loss \mathcal{L}_{AUX} in the overall optimization objective.

Note that the reconstruction \mathbf{r} is independent of the mainstream of the autoencoder and has only indirect relations with the codeword \mathbf{c} . These indirect relations are reflected in the following aspects: both \mathbf{r} and \mathbf{c} are generated by querying the same transformer model, and the embeddings corresponding to \mathbf{r} and \mathbf{c} may have interactions when applying the attention mechanism of the transformer. In view of this, we infer that the auxiliary reconstruction loss may be crucial to initiate the training of the autoencoder, and after this initiation, the weight μ may not have a significant impact on the overall performance.

Optimization of hyperparameter μ . We conducted experiments with different choices of the hyperparameter μ , which are $\mu = 0$ indicating the absence of the auxiliary reconstruction loss, and $\mu \in \{0.5, 1, 1.5\}$ for different weights for the auxiliary loss. Each column in Figure 5 corresponds to a choice of μ , and the curves of the validation NER and the cross-entropy loss between source and sink sequences are plotted against the training epochs.

The first column of Figure 5 indicates that without the auxiliary loss, all 5 runs of the training fail and produce random output. By comparing the first column with the other three, we can infer the effectiveness of introducing the auxiliary loss. In the subfigures corresponding to $\mu \in \{0.5, 1, 1.5\}$, all the models converge well, and the evaluation NERs also exhibit a similar convergence to a value of about 1%. From this, it may be inferred that the application of the auxiliary loss is essential, but the weight for the loss has little influence on the final performance.

Auxiliary loss on patterns beyond sequence reconstruction. After these experiments, a natural question arises: How about imparting the encoder with higher initial logical ability through a more complicated task rather than replication? Motivated by this, we adopted commonly used operations from existing IDS-correcting codes and attempted to recover the sequence from these operations using the encoder. In practice, we employed the forward difference $\text{Diff}(\mathbf{s})$, where

$$\text{Diff}(\mathbf{s})_i = s_i - s_{i+1} \pmod 4, \quad (9)$$

the position information-encoded sequence $\text{Pos}(\mathbf{s})$, where

$$\text{Pos}(\mathbf{s})_i = s_i + i \pmod 4, \quad (10)$$

and their combinations as the reconstructed sequences.

The evaluation NERs against training epochs are plotted in Figure 6 under different combinations of the identity mapping I, Diff, and Pos. It is clear that the reconstruction of the identity mapping I outperforms Diff and Pos. Among the combinations, I + Pos exhibits the best performance, while I + Diff + Pos performs the worst. These variations may be attributed to the capabilities of the transformers in our setting or the disordered implicit timings during training.

References

- [1] G. M. Church, Y. Gao, and S. Kosuri, "Next-generation digital information storage in DNA," *Science*, vol. 337, no. 6102, pp. 1628–1628, 2012.
- [2] N. Goldman, P. Bertone, S. Chen, C. Dessimoz, E. M. LeProust, B. Sipos, and E. Birney, "Towards practical, high-capacity, low-maintenance information storage in synthesized DNA," *Nature*, vol. 494, no. 7435, pp. 77–80, 2013.
- [3] R. N. Grass, R. Heckel, M. Puddu, D. Paunescu, and W. J. Stark, "Robust chemical preservation of digital information on DNA in silica with error-correcting codes," *Angewandte Chemie International Edition*, vol. 54, no. 8, pp. 2552–2555, 2015.
- [4] Y. Erlich and D. Zielinski, "DNA Fountain enables a robust and efficient storage architecture," *Science*, vol. 355, no. 6328, pp. 950–954, 2017.
- [5] L. Organick, S. D. Ang, Y.-J. Chen, R. Lopez, S. Yekhanin, K. Makarychev, M. Z. Racz, G. Kamath, P. Gopalan, B. Nguyen, *et al.*, "Random access in large-scale DNA data storage," *Nature Biotechnology*, vol. 36, no. 3, pp. 242–248, 2018.

- [6] Y. Dong, F. Sun, Z. Ping, Q. Ouyang, and L. Qian, “DNA storage: research landscape and future prospects,” *National Science Review*, vol. 7, pp. 1092–1107, 01 2020.
- [7] W. Chen, M. Han, J. Zhou, Q. Ge, P. Wang, X. Zhang, S. Zhu, L. Song, and Y. Yuan, “An artificial chromosome for data storage,” *National Science Review*, vol. 8, p. nwab028, 02 2021.
- [8] A. El-Shaikh, M. Welzel, D. Heider, and B. Seeger, “High-scale random access on DNA storage systems,” *NAR Genomics and Bioinformatics*, vol. 4, p. lqab126, 01 2022.
- [9] M. Blawat, K. Gaedke, I. Hütter, X.-M. Chen, B. Turczyk, S. Inverso, B. W. Pruitt, and G. M. Church, “Forward error correction for DNA data storage,” *Procedia Computer Science*, vol. 80, pp. 1011 – 1022, 2016. International Conference on Computational Science 2016, ICCS 2016, 6-8 June 2016, San Diego, California, USA.
- [10] D. Bar-Lev, T. Etzion, and E. Yaakobi, “On the size of balls and anticodes of small diameter under the fixed-length levenshtein metric,” *IEEE Transactions on Information Theory*, vol. 69, no. 4, pp. 2324–2340, 2023.
- [11] K. Cai, Y. M. Chee, R. Gabrys, H. M. Kiah, and T. T. Nguyen, “Correcting a single indel/edit for DNA-based data storage: Linear-time encoders and order-optimality,” *IEEE Transactions on Information Theory*, vol. 67, no. 6, pp. 3438–3451, 2021.
- [12] W. H. Press, J. A. Hawkins, S. K. Jones, J. M. Schaub, and I. J. Finkelstein, “HEDGES error-correcting code for DNA storage corrects indels and allows sequence constraints,” *Proceedings of the National Academy of Sciences*, vol. 117, no. 31, pp. 18489–18496, 2020.
- [13] P. Baldi, “Autoencoders, unsupervised learning, and deep architectures,” in *Proceedings of ICML workshop on unsupervised and transfer learning*, pp. 37–49, JMLR Workshop and Conference Proceedings, 2012.
- [14] T. Richardson and R. Urbanke, *Modern coding theory*. Cambridge university press, 2008.
- [15] Y. Choukroun and L. Wolf, “Error correction code transformer,” in *Advances in Neural Information Processing Systems* (S. Koyejo, S. Mohamed, A. Agarwal, D. Belgrave, K. Cho, and A. Oh, eds.), vol. 35, pp. 38695–38705, Curran Associates, Inc., 2022.
- [16] H. Kim, Y. Jiang, R. B. Rana, S. Kannan, S. Oh, and P. Viswanath, “Communication algorithms via deep learning,” in *International Conference on Learning Representations*, 2018.
- [17] Y. Jiang, H. Kim, H. Asnani, S. Kannan, S. Oh, and P. Viswanath, “Turbo autoencoder: Deep learning based channel codes for point-to-point communication channels,” in *Advances in Neural Information Processing Systems*, pp. 2754–2764, 2019.
- [18] A. Vaswani, N. Shazeer, N. Parmar, J. Uszkoreit, L. Jones, A. N. Gomez, L. u. Kaiser, and I. Polosukhin, “Attention is all you need,” in *Advances in Neural Information Processing Systems 30* (I. Guyon, U. V. Luxburg, S. Bengio, H. Wallach, R. Fergus, S. Vishwanathan, and R. Garnett, eds.), pp. 5998–6008, Curran Associates, Inc., 2017.
- [19] F. Kossentini, M. J. Smith, and C. F. Barnes, “Entropy-constrained residual vector quantization,” in *1993 IEEE International Conference on Acoustics, Speech, and Signal Processing*, vol. 5, pp. 598–601, IEEE, 1993.
- [20] R. R. Varshamov and G. Tenenholz, “A code for correcting a single asymmetric error,” *Automatica i Telemekhanika*, vol. 26, no. 2, pp. 288–292, 1965.
- [21] V. I. Levenshtein, “Binary codes capable of correcting deletions, insertions, and reversals,” *Soviet Physics. Doklady*, vol. 10, pp. 707–710, 1965.
- [22] L. Calabi and W. Hartnett, “A family of codes for the correction of substitution and synchronization errors,” *IEEE Transactions on Information Theory*, vol. 15, no. 1, pp. 102–106, 1969.
- [23] E. Tanaka and T. Kasai, “Synchronization and substitution error-correcting codes for the levenshtein metric,” *IEEE Transactions on Information Theory*, vol. 22, no. 2, pp. 156–162, 1976.
- [24] N. J. Sloane, “On single-deletion-correcting codes,” *Codes and designs*, vol. 10, pp. 273–291, 2000.

- [25] H. D. Pfister and I. Tal, “Polar codes for channels with insertions, deletions, and substitutions,” in *2021 IEEE International Symposium on Information Theory (ISIT)*, pp. 2554–2559, 2021.
- [26] Z. Yan, C. Liang, and H. Wu, “A segmented-edit error-correcting code with re-synchronization function for DNA-based storage systems,” *IEEE Transactions on Emerging Topics in Computing*, pp. 1–13, 2022.
- [27] M. Welzel, P. M. Schwarz, H. F. Löchel, T. Kabdullayeva, S. Clemens, A. Becker, B. Freisleben, and D. Heider, “DNA-Aeon provides flexible arithmetic coding for constraint adherence and error correction in DNA storage,” *Nature Communications*, vol. 14, no. 1, p. 628, 2023.
- [28] F. Sellers, “Bit loss and gain correction code,” *IRE Transactions on Information Theory*, vol. 8, no. 1, pp. 35–38, 1962.
- [29] B. Haeupler and A. Shahrasbi, “Synchronization strings and codes for insertions and deletions—a survey,” *IEEE Transactions on Information Theory*, vol. 67, no. 6, pp. 3190–3206, 2021.
- [30] M. Davey and D. Mackay, “Reliable communication over channels with insertions, deletions, and substitutions,” *IEEE Transactions on Information Theory*, vol. 47, no. 2, pp. 687–698, 2001.
- [31] M. Ibnkahla, “Applications of neural networks to digital communications—a survey,” *Signal Processing*, vol. 80, no. 7, pp. 1185–1215, 2000.
- [32] O. Simeone, “A very brief introduction to machine learning with applications to communication systems,” *IEEE Transactions on Cognitive Communications and Networking*, vol. 4, no. 4, pp. 648–664, 2018.
- [33] M. Akrouf, A. Feriani, F. Bellili, A. Mezghani, and E. Hossain, “Domain generalization in machine learning models for wireless communications: Concepts, state-of-the-art, and open issues,” *IEEE Communications Surveys & Tutorials*, 2023.
- [34] S. Cammerer, T. Gruber, J. Hoydis, and S. Ten Brink, “Scaling deep learning-based decoding of polar codes via partitioning,” in *GLOBECOM 2017-2017 IEEE Global Communications Conference*, pp. 1–6, IEEE, 2017.
- [35] E. Nachmani, E. Marciano, L. Lugosch, W. J. Gross, D. Burshtein, and Y. Be’ery, “Deep learning methods for improved decoding of linear codes,” *IEEE Journal of Selected Topics in Signal Processing*, vol. 12, no. 1, pp. 119–131, 2018.
- [36] E. Nachmani and L. Wolf, “Hyper-graph-network decoders for block codes,” in *Advances in Neural Information Processing Systems* (H. Wallach, H. Larochelle, A. Beygelzimer, F. d'Alché-Buc, E. Fox, and R. Garnett, eds.), vol. 32, Curran Associates, Inc., 2019.
- [37] A. V. Makkuva, X. Liu, M. V. Jamali, H. Mahdaviifar, S. Oh, and P. Viswanath, “Ko codes: inventing nonlinear encoding and decoding for reliable wireless communication via deep-learning,” in *International Conference on Machine Learning*, pp. 7368–7378, PMLR, 2021.
- [38] E. Balevi and J. G. Andrews, “Autoencoder-based error correction coding for one-bit quantization,” *IEEE Transactions on Communications*, vol. 68, no. 6, pp. 3440–3451, 2020.
- [39] S. Kullback, *Information theory and statistics*. Courier Corporation, 1997.
- [40] A. Van Den Oord, O. Vinyals, *et al.*, “Neural discrete representation learning,” *Advances in Neural Information Processing Systems*, vol. 30, 2017.
- [41] C. K. Sønderby, B. Poole, and A. Mnih, “Continuous relaxation training of discrete latent variable image models,” in *Bayesian Deep Learning workshop, NIPS*, vol. 201, 2017.
- [42] W. Williams, S. Ringer, T. Ash, D. MacLeod, J. Dougherty, and J. Hughes, “Hierarchical quantized autoencoders,” *Advances in Neural Information Processing Systems*, vol. 33, pp. 4524–4535, 2020.
- [43] C. E. Shannon, “A mathematical theory of communication,” *The Bell System Technical Journal*, vol. 27, no. 3, pp. 379–423, 1948.